THE JOURNAL OF BIOLOGICAL CHEMISTRY VOL. 287, NO. 23, pp. 19008–19017, June 1, 2012

Arabidopsis Vacuolar H^+-ATPase (V-ATPase) B Subunits Are Involved in Actin Cytoskeleton Remodeling via Binding to, Bundling, and Stabilizing F-actin*

Received for publication, July 12, 2011, and in revised form, February 24, 2012 Published, JBC Papers in Press, February 27, 2012, DOI 10.1074/jbc.M111.281873

Binyun Ma[1], **Dong Qian**[1], **Qiong Nan, Chang Tan, Lizhe An**[2], **and Yun Xiang**[3]
From the School of life Sciences, Lanzhou University, Lanzhou 730070, China

Vacuolar H^+-ATPase (V-ATPase) is a membrane-bound multisubunit enzyme complex composed of at least 14 different subunits. The complex regulates the physiological processes of a cell by controlling the acidic environment, which is necessary for certain activities and the interaction with the actin cytoskeleton through its B and C subunits in both humans and yeast. *Arabidopsis* V-ATPase has three B subunits (*At*VAB1, *At*VAB2, and *At*VAB3), which share 97.27% sequence identity and have two potential actin-binding sites, indicating that these *At*VABs may have crucial functions in actin cytoskeleton remodeling and plant cell development. However, their biochemical functions are poorly understood. In this study, we demonstrated that *At*VABs bind to and co-localize with F-actin, bundle F-actin to form higher order structures, and stabilize actin filaments *in vitro*. In addition, the *At*VABs also show different degrees of activities in capping the barbed ends but no nucleating activities, and these activities were not regulated by calcium. The functional similarity and differences of the *At*VABs implied that they may play cooperative and distinct roles in *Arabidopsis* cells.

Vacuolar H^+-ATPase (V-ATPase)[4] is a highly conserved, ATP-driven proton pump that is functionally and structurally related to the mitochondrial and chloroplast F-ATPase (1–3). V-ATPase is widely distributed in eukaryotic and prokaryotic cells and is responsible for proton transport across the plasma membrane and for the acidification of different intracellular organelles, including phagosomes, early endosomes, lysosomes, synaptosomes, the Golgi apparatus, clathrin-coated vesicles, dense core secretory granules, and plant vacuoles (4–6). In these organelles, V-ATPase is a multisubunit complex consisting of a water-soluble V1 subcomplex located in the cytosol, which catalyzes ATP binding and hydrolyzing, and a membrane-embedded V0 subcomplex containing the proton translocation pore that transports protons (6, 7). The peripheral V1 contains at least eight different subunits of molecular masses ranging between 13 and 70 kDa (subunits A, B, C, D, E, F, G, and H), whereas the membrane-integral V0 contains at least six different subunits of molecular masses ranging between 17 and 100 kDa (subunits a, c, c′, c″, d, and e) (6–9).

Recent studies have indicated that V-ATPase is directly involved in interactions with the actin cytoskeleton through actin-binding sites located in the N-terminal domain of subunit B (10–12) and in two domains of subunit C (13, 14). The B subunit N-terminal domains of plants, mammals, and yeast have a profilin-like motif that includes several conserved Gly, Leu, Val, Asp, and Phe residues (6, 10, 11) and conserved L(K/R)*XX*E(S/T)-like motifs. In the latter motifs, the conserved Leu, Arg, and Ser residues are identical to the L(K/R)*XX*E(S/T) motifs of several actin-binding proteins, including Dp71, PKCϵ, α-actinin, actobindin, and tropomyosin, in which Leu and Arg (or Lys) are crucial residues that can directly interact with the N terminus of actin (6). Thus, the V-ATPase B subunit may be involved in the dynamics of the actin cytoskeleton.

The actin cytoskeleton is a highly organized and dynamic structure present in all eukaryotic cells, where it plays a central role and is involved in numerous cellular processes, including intracellular transport, cell growth, cell division, cytoplasmic streaming, organelle positioning, and cell-to-cell communication (15–19). For such processes, a regulatory system is required that contains actin filaments and actin-binding proteins (ABPs) that directly interact with G-actin and/or F-actin to promote the nucleation, polymerization, depolymerization, stabilization, severing, capping, bundling, and cross-linking of actin filaments (20–23). Recently, some ABPs were proved to be involved in actin cytoskeleton remodeling, including *Arabidopsis* FIM5 (24), *Arabidopsis* VLN5 (25), tobacco WLIM1 (26), *Arabidopsis* LIM proteins (27), *Arabidopsis* VLN4 (28), and rice formin (29). These proteins have different activities in dynamic actin cytoskeleton remodeling and are involved in cell growth and development. In *Arabidopsis thaliana*, three V-ATPase B subunits (*At*VAB1, *At*VAB2, and *At*VAB3) (30–34) are expressed in different tissues and may play various functions in growth, differentiation, development, adaptation to changing environmental conditions, and maintenance of cell morphology (32, 35, 36). Nevertheless, how the B subunits of V-ATPase interact with actin filaments and regulate dynamic actin cytoskeleton remains poorly understood.

To understand the biochemical functions of *At*VABs *in vitro*, we first analyzed their structures based on homology molecular

* This work was supported by National Basic Research Program of China (973 Program) Grant 2007CB108902 and Chinese Transgenic Project Grant 2009ZX08009-029B (to L. A.), National Natural Science Foundation of China Grant 30800079, and China Postdoctoral Science Foundation Grant 200902311 (to Y. X.).
[1] Both authors contributed equally to this work.
[2] To whom correspondence may be addressed. E-mail: lizhean@lzu.edu.cn.
[3] To whom correspondence may be addressed. E-mail: xiangy@lzu.edu.cn.
[4] The abbreviations used are: V-ATPase, vacuolar H^+-ATPase; *At*VAB, *A. thaliana* V-ATPase B subunit; *At*VHA-Bs, *A. thaliana* vacuolar H^+-ATPase B subunit genes, including *At*VHA-B1 (*At*1g76030), -B2 (*At*4g38510), and -B3 (*At*1g20260); ABPs, actin-binding proteins; F-actin, filamental actin; G-actin, global actin; LatB, latrunculin B; TRITC, tetramethylrhodamine isothiocyanate.

modeling. The results indicated that polypeptides shared highly similar structures; however, an unconserved region and a novel residue among these subunits were found, suggesting that *At*VABs may have overlapping and distinct *in vitro* biochemical functions and *in vivo* physiological activities. The recombinant proteins were expressed in bacteria for the biochemical and microscopic analysis of their functions. Our findings strongly suggested that *At*VABs may act as actin-binding proteins and that they shared similar functional features with other reported ABPs.

EXPERIMENTAL PROCEDURES

Materials—Arabidopsis Columbia wild-type plants were used for total RNA extraction and cloning of the *At*VAB genes. Actin was isolated from an acetone extract from rabbit skeletal muscle according to previous methods (37). Monomeric actin was dialyzed in Buffer G (5.0 mM Tris-HCl, pH 8.0, 0.2 mM ATP, 0.5 mM DTT, 0.2 mM $CaCl_2$, and 0.01% sodium azide). Pyrene-actin was prepared by labeling actin at Cys^{374} with pyrene iodoacetamide as described previously for kinetic analyses (38). Human recombinant profilin I was purified as described previously (39). These proteins were frozen in liquid nitrogen and stored at −80 °C.

Preparation of Recombinant AtVABs and Specific Anti-AtVAB Antibody—Total *Arabidopsis* RNA was extracted from flowers using the Total RNA Isolation kit (TianGen). The cDNA coding sequences of *At*VAB1, *At*VAB2, and *At*VAB3 were amplified by RT-PCR using the specific primer pairs, $B1_F$/$B1_R$, $B2_F$/$B2_R$, and $B3_F$/BE_R (Table 1). The amplified fragments were cloned into the pMD19-T vector (TaKaRa), and the resulting cDNA sequences were verified by sequencing. The pGEX-*At*VAB1, pGEX-*At*VAB2, and pGEX-*At*VAB3 expression plasmids were constructed by cloning the *At*VAB coding sequences into the pGEX-4T-1 (GE Healthcare) vector after digestion at the BamHI and SacI restriction sites. The fusion proteins were then expressed in *Escherichia coli* BL21 (DE3) by induction with 0.5 mM isopropyl 1-thio-β-D-galactopyranoside overnight at 25 °C. Recombinant *At*VABs were affinity-purified using glutathione-Sepharose 4B resin (GE Healthcare) (the wash buffer was PBS (140 mM NaCl, 2.7 mM KCl, 10 mM $Na_2HPO_4{\cdot}12H_2O$, 1.8 mM KH_2PO_4, pH 7.4) and, with the proteins, were eluted with 50 mM Tris-HCl (pH 8.0) and 10 mM reduced glutathione. The purified proteins were concentrated in a centrifugal filter (Millipore), buffer-exchanged (10 mM Tris-HCl, 0.2 mM $CaCl_2$, 0.5 mM DTT, and 0.2 mM ATP, pH 7.4) using a 14 kDa molecular mass cut-off dialysis cassette (Pierce), and stored on ice. Prior to any experiments, the proteins were preclarified further by centrifugation at 100,000 × *g* for 1 h.

The purified recombinant *At*VAB2 was used as an antigen to raise anti-*At*VAB polyclonal antibodies in rabbit serum, as described by Huang *et al.* (40). The anti-*At*VAB polyclonal antibody was purified using an octanoic acid-saturated ammonium sulfate method. Rabbit antiserum (2 ml) was diluted 4-fold with 0.06 M HAc-NaAc buffer (pH 4.8), and octanoic acid was added dropwise into the diluted antiserum, whose final concentration reached 75 μl/ml; the mixture was stirred for 30 min. The mixture was centrifuged at 12,000 rpm for 20 min at room temperature; 0.01 M PBS (pH 7.4) was added to the supernatant, and then isopycnic saturated ammonium sulfate (pH 7.4) was gently added with stirring. The mixture was centrifuged at 12,000 rpm for 30 min at 4 °C and allowed to stand for 2 h. The pellet was dissolved and dialyzed in 0.01 M PBS (pH 7.4) overnight at 4 °C. The purified anti-*At*VAB2 antibody was used for Western blot analysis.

Immunofluorescence Labeling—In vitro immunofluorescence labeling was employed to test whether the *At*VABs co-localized with F-actin. Prepolymerized F-actin (3.0 μM) was incubated with 2.0 μM *At*VAB1, *At*VAB2, and *At*VAB3, respectively, for 1 h at 22 °C. Alexa-488 phalloidin-stabilized F-actin and TRITC-conjugated goat anti-rabbit IgG (H+L) (1:200)-stained *At*VABs were visualized using a Leica DFC420C microscope equipped with a ×100 objective and a CCD camera. The F-actin and TRITC-conjugated goat anti-rabbit IgG alone were included as negative controls. Merged images were acquired using Image-Pro Plus 6.0 (version 6.0.0.260; Media Cybernetics).

High and Low Speed Co-sedimentation Assays—High and low speed co-sedimentation assays were used to assess the actin-binding, -bundling, and -stabilizing activities of the *At*VABs.

The high speed co-sedimentation assays were initially employed to determine the activity of *At*VAB binding to F-actin, as described by Khurana *et al.* (41). Preassembled F-actin (5.0 μM) was incubated with 0.5 or 2.0 μM *At*VABs, GST (as a negative control) or ABP29 (as a positive control) (42) for 1 h at 22 °C, and the samples were centrifuged at 100,000 × *g* for 1 h at 4 °C (CS120GXII, Hitachi). After centrifugation, the supernatant and pellet fractions were resolved on SDS-polyacrylamide gels and stained with Coomassie Brilliant Blue. The intensities of the resulting bands were quantified densitometrically using Quantity One software (version 4.6.2; Bio-Rad). For the statistical analysis to characterize the ability of the *At*VABs to bind to F-actin, we used Student's *t* test of SPSS Statistics 17.0.

Additionally, high speed co-sedimentation assays were also employed to assess the F-actin-stabilizing activity of the *At*VABs with a 20 μM LatB treatment. Preformed F-actin (5.0 μM) was incubated with 0, 0.5, or 5.0 μM *At*VABs and GST (as a negative control) at 22 °C for 1 h prior to treatment with 20 μM LatB for 6 h. As another negative control, the F-actin was incubated and treated without the *At*VABs and LatB. As a positive control, the F-actin was incubated without the *At*VABs but treated with 20 μM LatB. The samples were centrifuged at 100,000 × *g* for 1 h, and the resulting pellets and supernatants were analyzed by SDS-PAGE. After quantification, the results were expressed as the percentage of actin in the supernatant as a function of the *At*VAB concentration. Statistical analysis was performed as described above.

Low speed sedimentation experiments were used to assess the actin bundling activity of the *At*VABs. Preassembled F-actin (5.0 μM) was incubated with 0, 0.5, or 2.0 μM *At*VABs and ABP29 (as a negative control) (42) in the presence of 200.0 μM calcium for 1 h at 22 °C. The samples were centrifuged at 13,500 × *g* for 30 min in a microcentrifuge at 4 °C to pellet the F-actin. The presence of actin in the resulting supernatants (nonbundled F-actins) and pellets (bundled F-actins) was analyzed by SDS-PAGE as described above. After quantification,

TABLE 1
Primers used in this study
The restriction enzyme sites are underlined. Start and stop codons are highlighted by boldface letters. F and for., forward primer; R and rev., reverse primer.

Primer name	Primer sequence	Purpose and restriction sites
$B1_F$	GGTACCGGATCCATGGGGACGAATGATCTCGACAT	*At*VAB1 cds for. KpnI/BamHI
$B1_R$	GAGCTCTTAACTGGTTGAGTCGCGGCTGT	*At*VAB1 cds rev. SacI
$B2_F$	GGATCCATGGGTGCTGCTGAAAACAACCT	*At*VAB2 cds for. BamHI
$B2_R$	GAGCTCTCAGTTGGTGGTATCGCGACTGT	*At*VAB2 cds rev. SacI
$B3_F$	GGTACCGGATCCATGGTGGAGACTAGTATCGACAT	*At*VAB3 cds for. KpnI/BamHI
$B3_R$	GAGCTCTTAGCTTGTGGAGTCGCGGCTGT	*At*VAB3 cds rev. SacI

the results were expressed as the percentage of actin in the pellet as a function of the *At*VAB concentration.

Fluorescence Microscopy Visualization of Actin Filaments and Bundles—Fluorescence microscopy was used to visualize the bundling activity of the *At*VABs. Prepolymerized actin (3.0 μM) was incubated with or without 2.0 μM *At*VABs for 1 h and labeled with 200 nM Alexa-488 phalloidin for 5 min at room temperature. The actin filaments were then diluted 10-fold with 1× F buffers (10× stock: 50 mM Tris-HCl, 5 mM ATP, 10 mM DTT, 0.5 M KCl, and 50 mM $MgCl_2$). A 1-μl aliquot of the diluted sample was used to visualize the actin filaments and bundles. Micrographs of the filament bundles were obtained using a Leica DFC420C fluorescence microscope equipped with a ×100 objective, a CCD camera, and Leica Application Suite software.

Actin Polymerization Assay—Actin nucleation assays were essentially employed according to a method described previously (42). Monomeric actin (5.0 μM; 5% pyrene-labeled) was incubated with various concentrations of *At*VABs for 5 min in the presence of 0.1 μM (treated with 1 mM EGTA) (42, 43), 10.0 μM (treated with 0.2 mM EGTA) (42, 43), or 200.0 μM free Ca^{2+} at room temperature. The polymerization of actin filaments was detected for 400 s by pyrene fluorescence with a FluoroMax®-4 spectrofluorometer immediately after the addition of one-tenth volume of 10× F buffers. The experiments were repeated at least three times under the same conditions.

Barbed End-capping Assay—To determine whether *At*VAB1, *At*VAB2, and *At*VAB3 cap the barbed end of actin filaments, a seeded elongation assay was performed as described previously (25). Preformed F-actin at a final concentration of 0.4 μM was incubated with various concentrations of the *At*VABs in the presence of 0.1 μM (treated with 1 mM EGTA) (42, 43), 10.0 μM (treated with 0.2 mM EGTA) (42, 43), or 200.0 μM free Ca^{2+} for 5 min at room temperature. Then 1 μM G-actin (5% pyrene-labeled) saturated with 4 μM human profilin I was added to the actin filament mixture. One-tenth volume of 10×F buffer was added to initiate actin elongation at the barbed end of the actin filaments. The time course of actin elongation was tracked by monitoring the increase of pyrene fluorescence with a FluoroMax®-4 spectrofluorometer, with the excitation wavelength set at 365 nm and emission wavelength at 407 nm after the actin elongation was initiated.

Actin Filament Depolymerization Assay—To test the effect of the *At*VABs on actin depolymerization, a depolymerization assay was performed, roughly according to a described method (42). Preassembled 5 μM F-actin (50% pyrene-labeled) was incubated with various concentrations of the *At*VABs in the presence of 200.0 μM free Ca^{2+} for 5 min at room temperature. Depolymerization was initiated by diluting the mixtures 25-fold with low ionic strength buffer G (5.0 mM Tris-HCl, pH 8.0, 0.2 mM ATP, 0.5 mM DTT, 0.2 mM $CaCl_2$, and 0.01% sodium azide). The decrease in pyrene fluorescence intensity accompanying the actin depolymerization was monitored over 400 s at room temperature using a FluoroMax®-4 spectrofluorometer (HORIBA Jobin Yvon). The experiments were repeated at least three times under the same conditions.

RESULTS

Binding and Co-localization between AtVABs and Actin Cytoskeleton in Vitro—Using the primer pairs $B1_F/B1_R$, $B2_F/B2_R$, and $B3_F/B3_R$ (Table 1), the full-length cDNAs of *At*VAB1, *At*VAB2, and *At*VAB3 were generated by RT-PCR. We found that the three subunits share high sequence identity (prediction identity = 97.27%) and that there was a conserved profilin-like actin-binding motif within each subunit (Fig. 1*A*), which shared a high identity with previously reported motifs (6, 10, 11). Several conserved residues (Gly^{37}, Leu^{39}, Val^{40}, Asp^{43}, and Lys^{44} in *At*VAB1 and *At*VAB3, Gly^{38}, Leu^{40}, Val^{41}, Asp^{44}, and Lys^{45} in *At*VAB2) were also found in yeast and humans. We considered that the *At*VABs can bind to F-actin through their profilin-like motifs located on the N-terminal β-barrel domain, an actin-binding region composed of 44 amino acids that are required for high affinity F-actin binding (11) (Fig. 1*A*). The recombinant *At*VABs and rabbit skeletal muscle actin were purified for the investigation of the interaction of *At*VABs with F-actin (filamentous actin) (Fig. 1*B*).

To test the hypothesis of the *At*VABs binding to F-actin, a high speed co-sedimentation assay was performed in the presence of 0.5 and 2.0 μM *At*VAB1, *At*VAB2, and *At*VAB3, respectively (Fig. 1*C*). The results showed that *At*VAB1, *At*VAB2, and *At*VAB3 bound to and co-sedimented with actin filaments (5.0 μM) (when centrifuged at 100,000 × *g* at 4 °C for 1 h) in a dose-dependent manner but that their abilities to bind to F-actin were similar. ABP29, a positive control, bound to F-actin as reported previously (42) (Fig. 1*D*), indicating that the *At*VABs can bind to F-actin with similar affinity *in vitro*.

To determine whether the *At*VABs and actin filaments co-localize, immunofluorescence labeling experiments were employed *in vitro*. The co-localization between the *At*VABs and actin filaments was observed when the *At*VABs were incubated with Alexa-488 phalloidin-stabilized F-actin (shown in *green*) and then labeled with an anti-*At*VAB antibody followed by TRITC-conjugated goat anti-rabbit IgG (shown in *red*) (Fig. 1*E*); no co-localization was detected when labeling was performed with the secondary antibody alone (data not shown). Taken together, these results suggested that *At*VAB1, *At*VAB2,

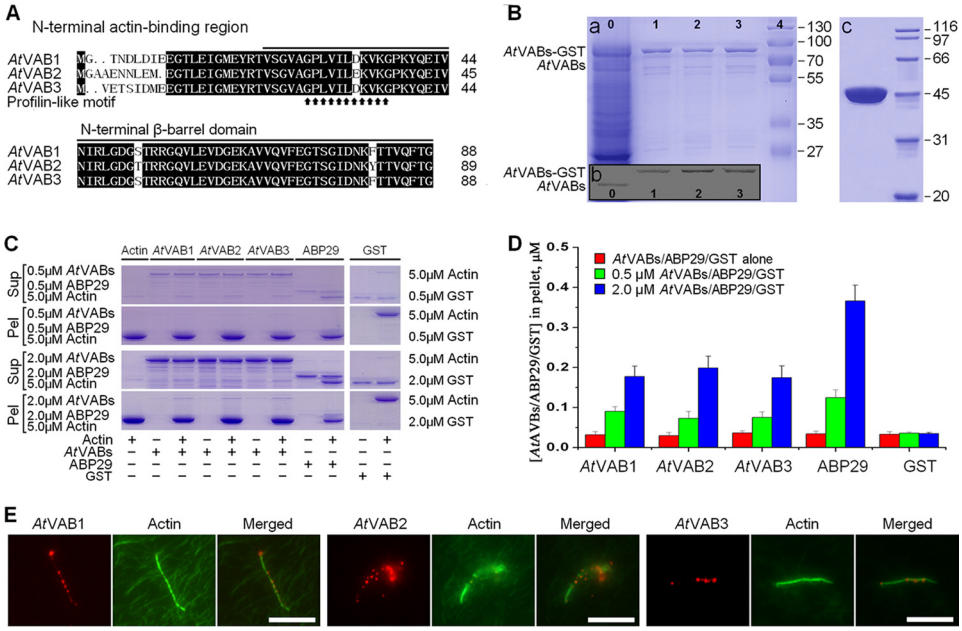

FIGURE 1. **Actin-binding domain and activity of *At*VABs binding to actin filaments.** *A*, the profilin-like motifs in the N-terminal β-barrel domains of *At*VAB1, *At*VAB2, and *At*VAB3 are indicated with *arrows*. *B*, total extract from *Arabidopsis* flowers; recombinant GST-*At*VAB1, -*At*VAB2, and -*At*VAB3; and rabbit skeletal muscle G-actin. *a*, *lane 0*, total extract from *Arabidopsis* flowers; *lanes 1–3*, GST-*At*VAB1, GST-*At*VAB2, and GST-*At*VAB3, respectively, with molecular masses of ~86 kDa; *lane 4*, molecular mass marker. *b*, protein immunoblots probed with anti-*At*VAB. *Lane 0*, 50 μg of total extract from *A. thaliana* flowers; *lanes 1–3*, GST-*At*VAB1, -*At*VAB2, and -*At*VAB3. *c*, G-actin was extracted from acetone powder from rabbit skeletal muscle. *C*, a high co-sedimentation assay was used to assess *At*VABs binding to F-actin (formed from 5.0 μM G-actin) centrifuged at 100,000 × *g*, 4 °C for 1 h. ABP29, a 29-kDa actin-binding protein, was used as a positive control. GST was used as a negative control. *Sup*, supernatant; *Pel*, pellet. *D*, statistical analysis of the AtVABs/ABP29/GST in pellet, which is shown in *C* ($n = 3$). *Bars*, mean ± S.E. (*error bars*) based on Student's *t test*. *E*, *At*VABs co-localize with the actin cytoskeleton *in vitro*, as performed with immunofluorescence labeling experiments. *At*VAB1, *At*VAB2, and *At*VAB3 were incubated with Alexa-488 phalloidin-stabilized F-actin (shown in *green*) and then stained with anti-*At*VAB2 antibody followed by TRITC-conjugated goat anti-rabbit IgG (shown in *red*), respectively. *Bars*, 100 μm.

and *At*VAB3 bound directly to F-actin in a beadlike manner *in vitro*.

AtVABs Bundle Actin Filaments in Vitro—To test whether *At*VABs are capable of generating actin filament bundles *in vitro*, a battery of biochemical and fluorescence microscopy assays were performed.

The ability of the *At*VABs to bundle F-actin to form a higher order structure was initially examined with a low speed co-sedimentation assay. Actin (5.0 μM) was polymerized alone or in the presence of 0.5 and 2.0 μM *At*VABs and centrifuged for 1 h at 13,500 × *g* at 4 °C (Fig. 2*A*). Because individual actin filaments were not sedimented at 13,500 × *g*, there should be appreciable actin in the pellet only in the presence of an actin-binding protein that is capable of bundling or cross-linking the filaments into networks. When incubated in the absence of the *At*VABs, very little polymerized actin was sedimented. In contrast, in the presence of each *At*VAB, the amount of actin in the pellet increased proportionally with the *At*VAB concentration. As reported previously (42), the ABP29 has no obvious F-actin bundling activity (Fig. 2*B*).

To further confirm the formation of the higher order structure, fluorescence light microscopy was employed to visualize the bundling activity of the *At*VABs. Prepolymerized actin (3.0 μM) was incubated with 2.0 μM *At*VABs for 1 h and labeled with 1 μM Alexa-488 phalloidin for 5 min at room temperature (Fig. 2, *C–F*). In the absence of the *At*VABs, the Alexa-488 phalloidin-labeled actin filaments formed a unitary meshwork of fine filaments (Fig. 2*C*). Conversely, when F-actin was incubated in the presence of each *At*VAB, agglomerate and network actin filament bundles were detected (Fig. 2, *D–F*), although single actin filaments were still present, indicating that all of the *At*VABs have the activity of bundling F-actin to form higher order, actin-based structures *in vitro*.

AtVABs Are Not Involved in Actin Polymerization in Vitro—To analyze the effects of *At*VABs on actin polymerization, the polymerization of the pyrene-labeled actin was monitored over time in the presence of various concentrations of *At*VAB1, *At*VAB2, or *At*VAB3 (Fig. 3*A–3C*). The polymerization rate of F-actin at the initial stage did not display obvious changes in the presence of *At*VAB1 (Fig. 3*A*), *At*VAB2 (Fig. 3*B*), or *At*VAB3 (Fig. 3*C*). As a positive control, ABP29 (0.5 μM) displayed a markedly promoted effect, as reported previously (42). As shown in Fig. 3, *D–F*, compared with the assays in the presence of 200.0 μM free Ca^{2+}, the actin polymerization mediated by *At*VABs was not affected by Ca^{2+} at the initial stage in the presence of 0.1 and 10.0 μM free Ca^{2+}, indicating that the nucleating activity of *At*VAB1, *At*VAB2, and AtVAB3 may not be regulated by Ca^{2+}.

AtVABs Cap Barbed Ends of Actin Filaments in Ca^{2+}-insensitive Manner—Many ABPs with capping activity bind to the barbed end of actin filaments with high affinity and prevent subunit addition and loss (44, 45). To determine whether *At*VAB1, *At*VAB2, and *At*VAB3 cap the barbed end of actin filaments, a seeded actin elongation assay was performed (40, 46). Preformed F-actin (0.4 μM) was incubated with varying concentrations of *At*VAB1, *At*VAB2, and *At*VAB3 for 5 min, and polymerization was initiated with the addition of 1 μM G-actin (5% pyrene-labeled) at a free Ca^{2+} of 0.1, 10.0, and

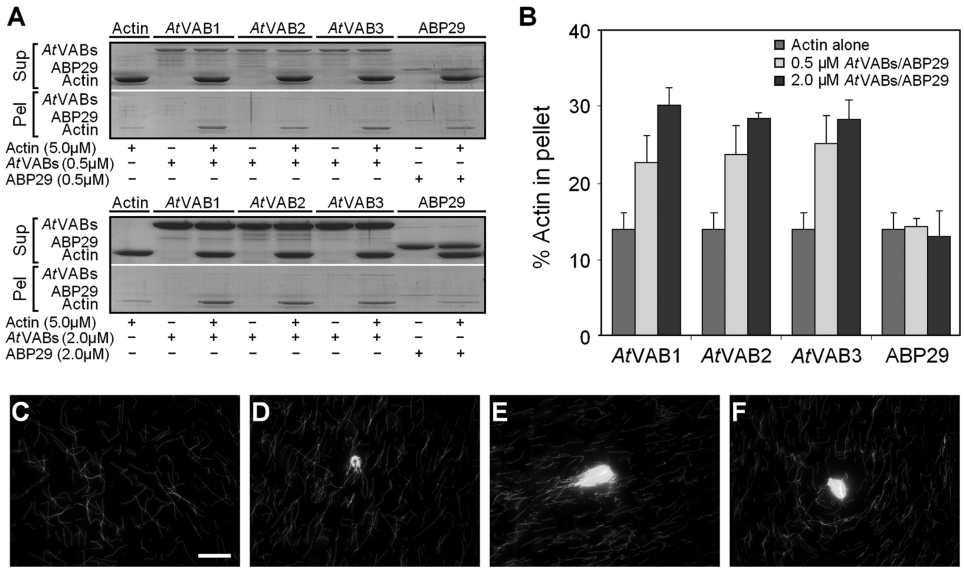

FIGURE 2. **AtVAB1, *At*VAB2, and *At*VAB3 bundle actin filaments *in vitro*.** *A*, a low speed co-sedimentation assay was performed to determine the bundling activity of the *At*VABs. Prepolymerized actin (5.0 μM) was incubated for 1 h with 0.5 and 2.0 μM *At*VAB1, *At*VAB2, *At*VAB3, and ABP29 (as a negative control), respectively. Then the mixtures were centrifuged at 13,500 $\times$ *g* for 1 h to separate the bundled *versus* unbundled actin filaments. After centrifugation, equal amounts of supernatant (*Sup*) and pellet (*Pel*) were separated by SDS-PAGE. *B*, *At*VABs bundled actin filaments in a dose-dependent manner, but ABP29 had no bundling actin filament activity. The *graph* shows the percentage of sedimented actin in *A* ($n = 3$). *Bars*, mean $\pm$ S.E. (*error bars*) based on Student's *t test*. *C–F*, fluorescence microscopy was performed to determine the bundling activity of *At*VAB1, *At*VAB2, and *At*VAB3. F-actin (3.0 μM) was incubated for 1 h with 2.0 μM *At*VAB1, *At*VAB2, and *At*VAB3, respectively, and subsequently labeled with 1 μM Alexa-488 phalloidin for 5 min at room temperature. Micrographs of actin bundles captured using fluorescence microscopy showed filament bundles. *C*, micrographs of actin filaments in the absence of *At*VAB1, *At*VAB2, and *At*VAB3. *D–F*, micrographs of actin filaments in the presence of 2.0 μM *At*VAB1, *At*VAB2, and *At*VAB3, respectively.

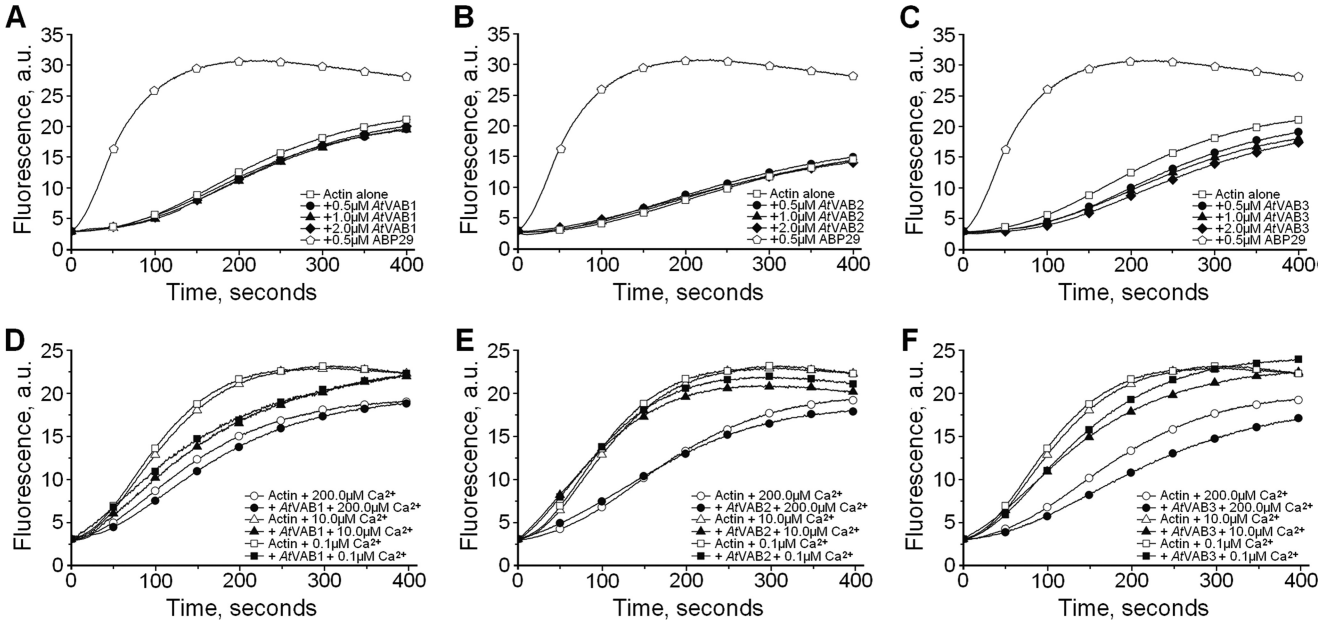

FIGURE 3. **Effect of *At*VABs on actin filament polymerization in a Ca^{2+}-insensitive manner.** Actin polymerization was performed with 5.0 μM actin (5% pyrene-labeled actin) in the presence of various concentrations of *At*VABs (0, 0.5, 1.0, and 2.0 μM), and various concentrations of free Ca^{2+} (0.1, 10.0, and 200.0 μM). ABP29 (0.5 μM) was used as a positive control. The time course of actin polymerization was recorded by measuring the pyrene fluorescence (arbitrary units (*a.u.*)), which was plotted *versus* time after the addition of polymerization salts to initiate the polymerization. *A–C*, various concentrations of *At*VABs and ABP29 were incubated for 5 min with 5.0 μM actin (5% pyrene-labeled actin) in the presence of 200.0 μM free Ca^{2+}. *D–F*, *At*VABs (2.0 μM) were incubated with 5.0 μM F-actin (5% pyrene-labeled actin) for 5 min in the presence of 0.1, 10.0, and 200.0 μM free Ca^{2+}.

200.0 μM, respectively. The G-actin was saturated with 4 μM human profilin I to suppress nucleation and the addition of actin to the pointed ends of the filaments, which permits the addition at the barbed ends unless they are capped (46). As shown in Fig. 4*A*-4C, *At*VAB1, *At*VAB2, and *At*VAB3 decreased the initial rate of actin elongation, confirming their barbed end-capping activity, in which *At*VAB1 and *At*VAB2 capped the barbed ends of F-actin in a dose-dependent manner, and *At*VAB3 had a marked capping activity at various concentrations. As reported previously (42), ABP29 capped the barbed ends of F-actin when present at a low concentration (0.1 μM). Compared with the assays in the presence of 200.0 μM free Ca^{2+}, the activities of 0.5 μM *At*VABs capping the barbed ends of F-actin were not regulated in the presence of 0.1 and 10.0 μM

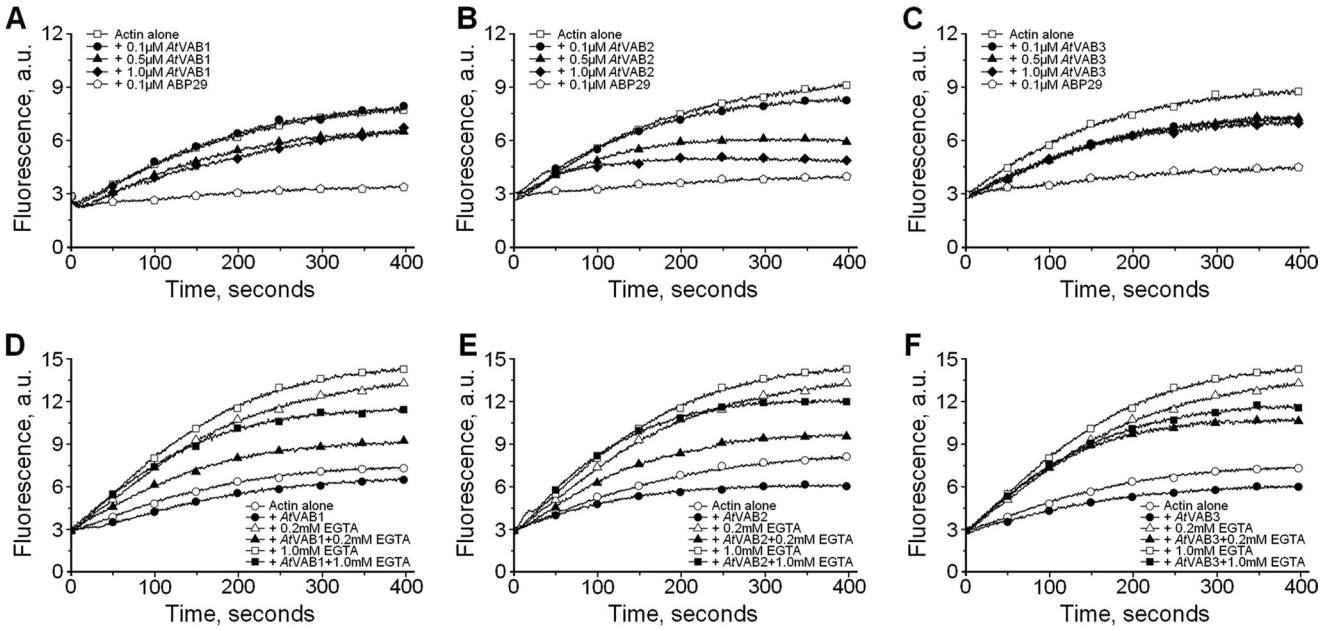

FIGURE 4. **AtVABs cap the barbed ends of actin filaments.** Preformed F-actin seeds (0.4 μM) were incubated with different concentrations of *At*VABs, and 1 μM G-actin, saturated with 4 μM human profilin I, was added to initiate actin elongation at the barbed end. Polymerization was monitored by tracking the increase in pyrene-actin fluorescence (arbitrary units (*a.u.*)) upon assembly. A single representative experiment ($n = 3$) is shown. *A–C*, various concentrations of *At*VAB1, *At*VAB2, and *At*VAB3 and 0.1 μM ABP29 (as a positive control) were incubated with 0.4 μM F-actin seeds in the presence of. 200.0 μM free Ca^{2+}. *D–F*, 0.5 μM *At*VAB1, *At*VAB2, and *At*VAB3 were incubated with 0.4 μM F-actin seeds in the presence of 0.1, 10.0, and 200.0 μM free Ca^{2+}.

free Ca^{2+} (Fig. 4, *D–F*). The monitored curve for each *At*VAB tracked with the corresponding actin control, indicating that the activity of *At*VAB1, *At*VAB2, and AtVAB3 capping the barbed ends of actin filaments may not be regulated by Ca^{2+}.

AtVABs Can Stabilize Actin Filaments in Vitro—To determine whether *At*VAB1, *At*VAB2, and *At*VAB3 stabilize actin filaments from depolymerization *in vitro*, we first used a high speed co-sedimentation assay with actin-depolymerizing latrunculin B (LatB) treatment (26). F-actin was polymerized alone or in the presence of various concentrations of recombinant *At*VAB1, *At*VAB2, *At*VAB3, or GST (as a negative control) and subsequently submitted to LatB treatment for 6 h (Fig. 5*A*). The samples were centrifuged at 100,000 × *g* for 1 h, and the amounts of actin in the resulting supernatants were quantified and expressed as a percentage of the total actin (Fig. 5*B*). As shown in Fig. 5*B*, less than 10% of the actin was detected in the supernatant of the control sample without LatB treatment, whereas 40% of the actin was detected in the supernatant with 20 μM LatB treatment in the absence of *At*VABs. The percentage of actin in the supernatant was significantly decreased proportionally in the presence of 0.5 and 5.0 μM *At*VAB1, *At*VAB2, and *At*VAB3 after 6 h of LatB treatment. Interestingly, *At*VAB1 and *At*VAB3 inhibited the depolymerization of the actin filaments induced by the LatB treatment in a dose-dependent manner, but *At*VAB2 did not. As a negative control, GST did not inhibit the depolymerization of the actin filaments induced by LatB (Fig. 5, *A* and *B*). These results indicated that *At*VAB1, *At*VAB2, and *At*VAB3 have distinct stabilizing activities on actin filaments *in vitro*.

The effect of *At*VABs on the actin filament depolymerization kinetics was also investigated by a dilution-mediated actin depolymerization assay using pyrene-labeled F-actin (26). In this assay, *At*VAB1 and *At*VAB3 inhibited depolymerization significantly (Fig. 5, *C* and *E*), whereas *At*VAB2 weakly inhibited actin depolymerization (Fig. 5*D*). In all of these assays, 0.5 μM ABP29 consistently markedly inhibited the actin depolymerization, as reported previously (42). These results further indicated that *At*VAB1, *At*VAB2, and *At*VAB3 have different activities for stabilizing actin filaments *in vitro*.

Taken together, these data suggested that actin polymerization/depolymerization may be regulated by *At*VAB1, *At*VAB2, and *At*VAB3 to varying degrees *in vivo*.

DISCUSSION

V-ATPases are ubiquitous proton pumps in eukaryotic cells that are responsible for the acidification of compartments of the endocytic and exocytic pathways (7). Previous reports indicated that V-ATPase may interact with microfilaments via both the B (10, 11) and C subunits (13, 14). The V-ATPases bind to F-actin (microfilaments) through actin-binding domains on the subunit B in mammalian cells (10), tobacco hornworm cells (13), and yeast cells (47). In mammalian and yeast cells, the B subunits bind to F-actin with high affinity (K_d = 130–195 nM), and a profilin-like motif composed of 11 amino acids is proven to be vital for this actin-binding activity because the F-actin-binding activity of the B subunit was inhibited when these 11 amino acids were deleted (10, 48). To date, it is not known whether the *Arabidopsis* V-ATPase B subunits also interact with F-actin.

AtVABs Share Overlapping Activities of Binding to and Bundling Filamentous Actin and Capping Barbed Ends of Actin Filaments—We analyzed the sequences of the V-ATPase B subunits from mammals, yeast, and *Arabidopsis* and found that there were two potential actin-binding domains, a profilin-like motif (6, 10, 11, 14) and L(K/R)*XX*E(S/T)-like motifs (6), among these B subunits. Therefore, we can propose a logical hypothe-

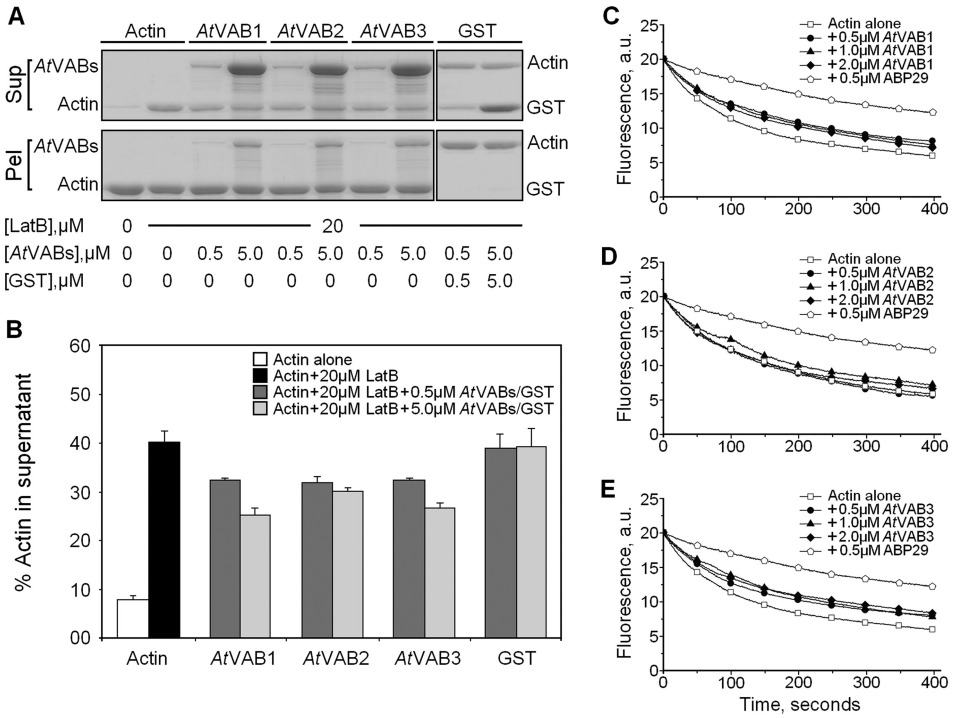

FIGURE 5. **AtVABs have the distinct ability to stabilize F-actin *in vitro*.** *A*, F-actin (5.0 μM) was incubated with 0, 0.5, and 5.0 μM *At*VABs and GST (as a negative control) for 1 h and subsequently treated without or with 20 μM LatB for 6 h. Samples were centrifuged at 100,000 $\times$ *g* for 1 h, and the resulting pellets (*Pel*) and supernatants (*Sup*) were analyzed by SDS-PAGE. *B*, statistical analysis of the results shown in *A* ($n = 3$) revealed that *At*VAB1, *At*VAB2, and *At*VAB3 inhibited the depolymerization of the actin filaments induced by the LatB treatment. *At*VAB1 and *At*VAB3 acted in a dose-dependent manner, whereas *At*VAB2 did not. *Bars*, mean $\pm$ S.E. (*error bars*) by Student's *t test*. *C–E*, dilution-mediated depolymerization assays were performed to determine the actin-stabilizing activities of *At*VABs. *At*VABs at various concentrations (0, 0.5, 1.0, and 2.0 μM) and ABP29 (0.5 μM) were incubated for 5 min with 5.0 μM F-actin (50% pyrene-labeled actin) in the presence of 200.0 μM free Ca^{2+}. Pyrene fluorescence (arbitrary units (*a.u.*)) was plotted *versus* time after the 25-fold dilution of the mixture with buffer G. In the representative experiment, *At*VAB1 and *At*VAB3 stabilized actin filaments from dilution-mediated depolymerization, but *At*VAB2 exhibited no marked activity.

sis of *At*VAB binding to F-actin. Our data also suggest that each of the *At*VABs can bind to actin filaments and that these subunits were co-localized along the elongating direction of F-actin.

The conservation of actin-binding domains in *At*VABs allowed us to predict that they may perform conserved actin-related functions, such as binding, bundling, capping, and stabilizing activities. F-actin bundling is generally mediated by proteins or protein complexes containing multiple actin-binding domains or two discrete actin-binding domains separated by longer distance (20). In fact, our low speed co-sedimentation and fluorescence microscopy assays unambiguously demonstrated that the *At*VABs bundled F-actin and induced the formation of high order actin structures.

Previous reports indicated that several classes of ABPs are known to control filament barbed ends both *in vitro* and *in vivo* (40, 49) and stabilize actin filaments by preventing subunit loss or addition at that end. These ABPs regulate the addition and loss of subunits from either the barbed (plus) or pointed (minus) ends of filaments; nucleating proteins initiate efficient actin polymerization and create new barbed ends for assembly. To determine whether *At*VABs cap actin filaments, a seeded actin elongation assay was employed. The results demonstrate that *At*VABs bind to the barbed end of actin filaments and prevent the addition of actin and the profilin-actin complex, confirming their capping activity. In addition, our data indicated that the capping of the filament barbed end activities of *At*VAB1, *At*VAB2, and *At*VAB3 were not regulated by free calcium.

In plant cells, the formation of higher order actin structures, such as bundles and cables, is crucial to stabilize the organization of transvacuolar strands and maintain the overall cellular architecture (50). As mentioned above, a subset of overlapping activities of *At*VABs may be involved in stabilizing long actin filaments. This result prompted us to investigate whether *At*VABs stabilize actin filaments directly. *In vitro* LatB treatment experiments and pyrene fluorescence assays indicated that *At*VABs stabilize actin filaments/bundles against LatB with distinct activity. Our data suggest that the actin filament-stabilizing activity may be regulated by *At*VAB1, *At*VAB2, and *At*VAB3 to varying degrees *in vivo*.

Molecular Bases of Distinct Activities of AtVABs—The results from our investigation on the activities of *At*VAB1, *At*VAB2, and *At*VAB3 in the regulation of actin cytoskeleton remodeling demonstrated differences among *At*VAB1, *At*VAB2, and *At*VAB3, despite the fact that these proteins share a high sequence identity (identity = 97.27%). We found a novel residue (Phe^{81} in *At*VAB1 and *At*VAB3 and Tyr^{82} in *At*VAB2) in the N-terminal β-barrel domain (Fig. 6*A*) and an unconserved region in the central α/β domains (Fig. 6*B*) that may result in the distinct activities of the *At*VABs.

To test this hypothesis, we reconstructed the three-dimensional structures of *At*VAB1, *At*VAB2, and *At*VAB3 based on the putative amino acid sequences by homology comparative

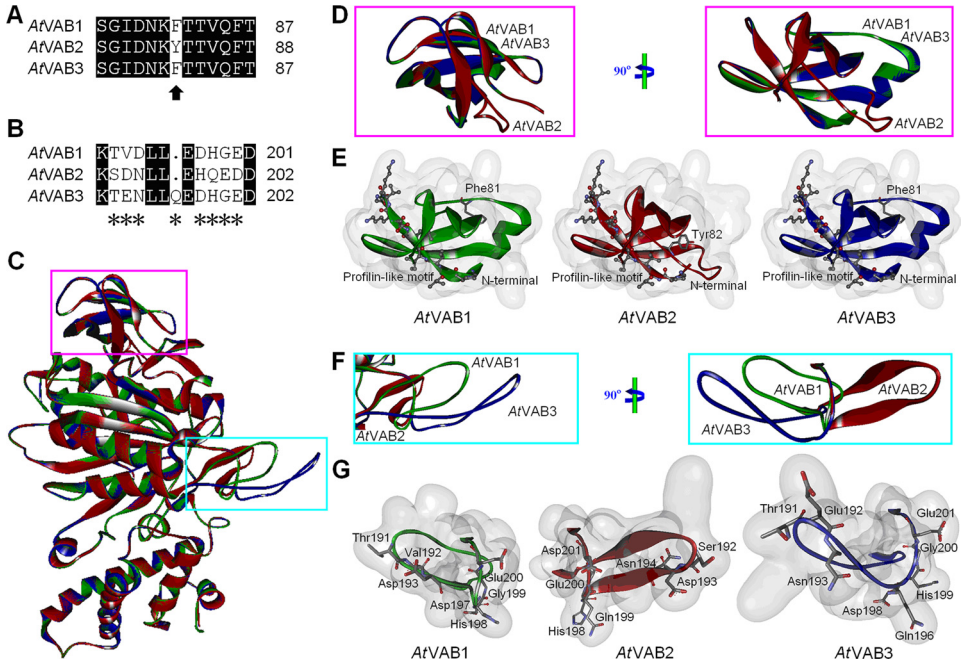

FIGURE 6. **Molecular structures and unconserved sites and regions of *At*VABs.** *A*, novel unconserved residues (indicated with an *arrow*) in the N-terminal β-barrel domains of *At*VABs: Phe[81] in *At*VAB1 and *At*VAB3 and Tyr[82] in *At*VAB2. *B*, sequence alignment of the unconserved regions in the central α/β domains of *At*VAB1, *At*VAB2, and *At*VAB3; the *asterisks* represent unconserved residues. *C*, molecular structures (*solid ribbon*) of the *At*VABs; the structures of *At*VAB1 (*green*), *At*VAB2 (*red*), and *At*VAB3 (*blue*) were superimposed onto each other. The β-barrel domains with the novel residues are indicated with a *fuchsia box*, and the unconserved regions are indicated with a *sky blue box*. *D*, structures of the β-barrel domains with the novel sites of *At*VAB1 (*green*), *At*VAB2 (*red*), and *At*VAB3 (*blue*). *E*, surface electrostatic potential of the β-barrel domains at the novel sites of *At*VAB1, *At*VAB2, and *At*VAB3 as in *D*. The unconserved residues are shown in *stick representations*. The conserved profilin-like motifs are shown in *ball-and-stick representations*. *F*, the structures of the unconserved regions of *At*VAB1 (*green*), *At*VAB2 (*red*), and *At*VAB3 (*blue*), showing the different spatial array. *G*, surface electrostatic potential in the unconserved regions of *At*VAB1, *At*VAB2, and *At*VAB3 as in *F*. The unconserved residues are shown in *stick representations*.

modeling. To confirm structural differences of the sites and regions, the structures of *At*VAB1, *At*VAB2, and *At*VAB3 were superimposed onto each other (Fig. 6*C*); the results indicated two distinct structural differences at the novel residues and the unconserved regions (Fig. 6, *D*–*G*). Compared with *At*VAB1 and *At*VAB3, the structure of *At*VAB2 displayed a great alteration due to Tyr[82] (Fig. 6*E*); in addition, the unconserved regions created distinct structures (Fig. 6*G*). These data suggested that the structural differences among *At*VAB1, *At*VAB2, and *At*VAB3 might form the basis for their distinct activities in the regulation of actin cytoskeleton dynamics.

The analysis of the expression level of the *At*VHA-B1, -B2, and -B3 genes using the e-FP Browser indicated that the three genes are expressed in all tissues in every developmental stage (51); however, the expression level of *At*VHA-B2 is lower than the other two. Specifically, in cauline leaves, rosette leaf 2, and stem (second internode), the GeneChip operating software expression signal of *At*VHA-B2 is markedly lower than *At*VHA-B1 and *At*VHA-B3. However, in mature pollen, the GeneChip operating software expression signal of *At*VHA-B2 is significantly higher than *At*VHA-B1 and *At*VHA-B3.

Taken together, the functional differences of *At*VAB1, *At*VAB2, and *At*VAB3 imply that they may be involved in different physiological processes of the same cell trafficking or different regulation pathways of different physiological processes, resulting in conserved heredity of *At*VAB1, *At*VAB2, and *At*VAB3 over the course of evolution in *A. thaliana*.

Acknowledgments—We thank Jia Li (Lanzhou University) for supplying the high speed centrifuge and Wenliang He (Lanzhou University) for technical assistance.

REFERENCES

1. Stock, D., Gibbons, C., Arechaga, I., Leslie, A. G., and Walker, J. E. (2000) The rotary mechanism of ATP synthase. *Curr. Opin. Struct. Biol.* **10,** 672–679
2. Yoshida, M., Muneyuki, E., and Hisabori, T. (2001) ATP synthase. A marvellous rotary engine of the cell. *Nat. Rev. Mol. Cell Biol.* **2,** 669–677
3. von Ballmoos, C., Wiedenmann, A., and Dimroth, P. (2009) Essentials for ATP synthesis by F_1F_0-ATP synthases. *Annu. Rev. Biochem.* **78,** 649–672
4. Kane, P. M. (2006) The where, when, and how of organelle acidification by the yeast vacuolar H^+-ATPase. *Microbiol. Mol. Biol. Rev.* **70,** 177–191
5. Forgac, M. (2007) Vacuolar ATPases. Rotary proton pumps in physiology and pathophysiology. *Nat. Rev. Mol. Cell Biol.* **8,** 917–929
6. Ma, B., Xiang, Y., and An, L. (2011) Structural bases of physiological functions and roles of the vacuolar H^+-ATPase. *Cell. Signal.* **23,** 1244–1256
7. Nishi, T., and Forgac, M. (2002) The vacuolar H^+-ATPases. Nature's most versatile proton pumps. *Nat. Rev. Mol. Cell Biol.* **3,** 94–103
8. Graham, L. A., Flannery, A. R., and Stevens, T. H. (2003) Structure and assembly of the yeast V-ATPase. *J. Bioenerg. Biomembr.* **35,** 301–312
9. Cipriano, D. J., Wang, Y., Bond, S., Hinton, A., Jefferies, K. C., Qi, J., and Forgac, M. (2008) Structure and regulation of the vacuolar ATPases. *Biochim. Biophys. Acta* **1777,** 599–604
10. Holliday, L. S., Lu, M., Lee, B. S., Nelson, R. D., Solivan, S., Zhang, L., and Gluck, S. L. (2000) The amino-terminal domain of the B subunit of vacuolar H^+-ATPase contains a filamentous actin binding site. *J. Biol. Chem.* **275,** 32331–32337
11. Chen, S. H., Bubb, M. R., Yarmola, E. G., Zuo, J., Jiang, J., Lee, B. S., Lu, M., Gluck, S. L., Hurst, I. R., and Holliday, L. S. (2004) Vacuolar H+-ATPase

binding to microfilaments. Regulation in response to phosphatidylinositol 3-kinase activity and detailed characterization of the actin-binding site in subunit B. *J. Biol. Chem.* **279,** 7988–7998
12. Breton, S., Wiederhold, T., Marshansky, V., Nsumu, N. N., Ramesh, V., and Brown, D. (2000) The B1 subunit of the H+ATPase is a PDZ domain-binding protein. Colocalization with NHE-RF in renal B-intercalated cells. *J. Biol. Chem.* **275,** 18219–18224
13. Vitavska, O., Merzendorfer, H., and Wieczorek, H. (2005) The V-ATPase subunit C binds to polymeric F-actin as well as to monomeric G-actin and induces cross-linking of actin filaments. *J. Biol. Chem.* **280,** 1070–1076
14. Vitavska, O., Wieczorek, H., and Merzendorfer, H. (2003) A novel role for subunit C in mediating binding of the H^+-V-ATPase to the actin cytoskeleton. *J. Biol. Chem.* **278,** 18499–18505
15. Staiger, C. J. (2000) Signaling to the actin cytoskeleton in plants. *Annu. Rev. Plant Physiol. Plant Mol. Biol.* **51,** 257–288
16. Palanivelu, R., and Preuss, D. (2000) Pollen tube targeting and axon guidance. Parallels in tip growth mechanisms. *Trends Cell Biol.* **10,** 517–524
17. Li, Y., Zee, S. Y., Liu, Y. M., Huang, B. Q., and Yen, L. F. (2001) Circular F-actin bundles and a G-actin gradient in pollen and pollen tubes of *Lilium davidii*. *Planta* **213,** 722–730
18. Kim, H., Park, M., Kim, S. J., and Hwang, I. (2005) Actin filaments play a critical role in vacuolar trafficking at the Golgi complex in plant cells. *Plant Cell* **17,** 888–902
19. Pollard, T. D., and Cooper, J. A. (2009) Actin, a central player in cell shape and movement. *Science* **326,** 1208–1212
20. Winder, S. J., and Ayscough, K. R. (2005) Actin-binding proteins. *J. Cell Sci.* **118,** 651–654
21. Pollard, T. D. (2007) Regulation of actin filament assembly by Arp2/3 complex and formins. *Annu. Rev. Biophys. Biomol. Struct.* **36,** 451–477
22. Oda, T., and Maéda, Y. (2010) Multiple conformations of F-actin. *Structure* **18,** 761–767
23. Bugyi, B., and Carlier, M. F. (2010) Control of actin filament treadmilling in cell motility. *Annu. Rev. Biophys.* **39,** 449–470
24. Wu, Y., Yan, J., Zhang, R., Qu, X., Ren, S., Chen, N., and Huang, S. (2010) *Arabidopsis* FIMBRIN5, an actin bundling factor, is required for pollen germination and pollen tube growth. *Plant Cell* **22,** 3745–3763
25. Zhang, H., Qu, X., Bao, C., Khurana, P., Wang, Q., Xie, Y., Zheng, Y., Chen, N., Blanchoin, L., Staiger, C. J., and Huang, S. (2010) *Arabidopsis* VILLIN5, an actin filament bundling and severing protein, is necessary for normal pollen tube growth. *Plant Cell* **22,** 2749–2767
26. Thomas, C., Hoffmann, C., Dieterle, M., Van Troys, M., Ampe, C., and Steinmetz, A. (2006) Tobacco WLIM1 is a novel F-actin-binding protein involved in actin cytoskeleton remodeling. *Plant Cell* **18,** 2194–2206
27. Papuga, J., Hoffmann, C., Dieterle, M., Moes, D., Moreau, F., Tholl, S., Steinmetz, A., and Thomas, C. (2010) *Arabidopsis* LIM proteins. A family of actin bundlers with distinct expression patterns and modes of regulation. *Plant Cell* **22,** 3034–3052
28. Zhang, Y., Xiao, Y., Du, F., Cao, L., Dong, H., and Ren, H. (2011) *Arabidopsis* VILLIN4 is involved in root hair growth through regulating actin organization in a Ca^{2+}-dependent manner. *New. Phytol.* **190,** 667–682
29. Yang, W., Ren, S., Zhang, X., Gao, M., Ye, S., Qi, Y., Zheng, Y., Wang, J., Zeng, L., Li, Q., Huang, S., and He, Z. (2011) BENT UPPERMOST INTERNODE1 encodes the class II formin FH5 crucial for actin organization and rice development. *Plant Cell* **23,** 661–680
30. Mayer, K. F., Schüller, C., Wambutt, R., Murphy, G., Volckaert, G., Pohl, T., Düsterhöft, A., Stiekema, W., Entian, K. D., Terryn, N., Ansorge, W., Brandt, P., Grivell, L., Rieger, M., Weichselgartner, M., de Simone, V., Obermaier, B., Mache, R., Müller, M., Kreis, M., Delseny, M., Puigdomenech, P., Watson, M., Schmidtheini, T., Reichert, B., Portatelle, D., Perez-Alonso, M., Boutry, M., Bancroft, I., Vos, P., Hoheisel, J., Zimmermann, W., Wedler, H., Ridley, P., Langham, S. A., McCullagh, B., Bilham, L., Robben, J., Van der Schueren, J., Grymonprez, B., Chuang, Y. J., Vandenbussche, F., Braeken, M., Weltjens, I., Voet, M., Bastiaens, I., Aert, R., Defoor, E., Weitzenegger, T., Bothe, G., Ramsperger, U., Hilbert, H., Braun, M., Holzer, E., Brandt, A., Peters, S., van Staveren, M., Dirske, W., Mooijman, P., Klein Lankhorst, R., Rose, M., Hauf, J., Kötter, P., Berneiser, S., Hempel, S., Feldpausch, M., Lamberth, S., Van den Daele, H., De Keyser, A., Buysshaert, C., Gielen, J., Villarroel, R., De Clercq, R., Van Montagu, M., Rogers, J., Cronin, A., Quail, M., Bray-Allen, S., Clark, L., Doggett, J., Hall, S., Kay, M., Lennard, N., McLay, K., Mayes, R., Pettett, A., Rajandream, M. A., Lyne, M., Benes, V., Rechmann, S., Borkova, D., Blöcker, H., Scharfe, M., Grimm, M., Löhnert, T. H., Dose, S., de Haan, M., Maarse, A., Schäfer, M., Müller-Auer, S., Gabel, C., Fuchs, M., Fartmann, B., Granderath, K., Dauner, D., Herzl, A., Neumann, S., Argiriou, A., Vitale, D., Liguori, R., Piravandi, E., Massenet, O., Quigley, F., Clabauld, G., Mündlein, A., Felber, R., Schnabl, S., Hiller, R., Schmidt, W., Lecharny, A., Aubourg, S., Chefdor, F., Cooke, R., Berger, C., Montfort, A., Casacuberta, E., Gibbons, T., Weber, N., Vandenbol, M., Bargues, M., Terol, J., Torres, A., Perez-Perez, A., Purnelle, B., Bent, E., Johnson, S., Tacon, D., Jesse, T., Heijnen, L., Schwarz, S., Scholler, P., Heber, S., Francs, P., Bielke, C., Frishman, D., Haase, D., Lemcke, K., Mewes, H. W., Stocker, S., Zaccaria, P., Bevan, M., Wilson, R. K., de la Bastide, M., Habermann, K., Parnell, L., Dedhia, N., Gnoj, L., Schutz, K., Huang, E., Spiegel, L., Sehkon, M., Murray, J., Sheet, P., Cordes, M., Abu-Threideh, J., Stoneking, T., Kalicki, J., Graves, T., Harmon, G., Edwards, J., Latreille, P., Courtney, L., Cloud, J., Abbott, A., Scott, K., Johnson, D., Minx, P., Bentley, D., Fulton, B., Miller, N., Greco, T., Kemp, K., Kramer, J., Fulton, L., Mardis, E., Dante, M., Pepin, K., Hillier, L., Nelson, J., Spieth, J., Ryan, E., Andrews, S., Geisel, C., Layman, D., Du, H., Ali, J., Berghoff, A., Jones, K., Drone, K., Cotton, M., Joshu, C., Antonoiu, B., Zidanic, M., Strong, C., Sun, H., Lamar, B., Yordan, C., Ma, P., Zhong, J., Preston, R., Vil, D., Shekher, M., Matero, A., Shah, R., Swaby, I. K., O'Shaughnessy, A., Rodriguez, M., Hoffmann, J., Till, S., Granat, S., Shohdy, N., Hasegawa, A., Hameed, A., Lodhi, M., Johnson, A., Chen, E., Marra, M., Martienssen, R., and McCombie, W. R. (1999) Sequence and analysis of chromosome 4 of the plant *Arabidopsis thaliana*. *Nature* **402,** 769–777
31. Theologis, A., Ecker, J. R., Palm, C. J., Federspiel, N. A., Kaul, S., White, O., Alonso, J., Altafi, H., Araujo, R., Bowman, C. L., Brooks, S. Y., Buehler, E., Chan, A., Chao, Q., Chen, H., Cheuk, R. F., Chin, C. W., Chung, M. K., Conn, L., Conway, A. B., Conway, A. R., Creasy, T. H., Dewar, K., Dunn, P., Etgu, P., Feldblyum, T. V., Feng, J., Fong, B., Fujii, C. Y., Gill, J. E., Goldsmith, A. D., Haas, B., Hansen, N. F., Hughes, B., Huizar, L., Hunter, J. L., Jenkins, J., Johnson-Hopson, C., Khan, S., Khaykin, E., Kim, C. J., Koo, H. L., Kremenetskaia, I., Kurtz, D. B., Kwan, A., Lam, B., Langin-Hooper, S., Lee, A., Lee, J. M., Lenz, C. A., Li, J. H., Li, Y., Lin, X., Liu, S. X., Liu, Z. A., Luros, J. S., Maiti, R., Marziali, A., Militscher, J., Miranda, M., Nguyen, M., Nierman, W. C., Osborne, B. I., Pai, G., Peterson, J., Pham, P. K., Rizzo, M., Rooney, T., Rowley, D., Sakano, H., Salzberg, S. L., Schwartz, J. R., Shinn, P., Southwick, A. M., Sun, H., Tallon, L. J., Tambunga, G., Toriumi, M. J., Town, C. D., Utterback, T., Van Aken, S., Vaysberg, M., Vysotskaia, V. S., Walker, M., Wu, D., Yu, G., Fraser, C. M., Venter, J. C., and Davis, R. W. (2000) Sequence and analysis of chromosome 1 of the plant *Arabidopsis thaliana*. *Nature* **408,** 816–820
32. Sze, H., Schumacher, K., Müller, M. L., Padmanaban, S., and Taiz, L. (2002) A simple nomenclature for a complex proton pump. VHA genes encode the vacuolar H^+-ATPase. *Trends Plant Sci.* **7,** 157–161
33. Shimaoka, T., Ohnishi, M., Sazuka, T., Mitsuhashi, N., Hara-Nishimura, I., Shimazaki, K., Maeshima, M., Yokota, A., Tomizawa, K., and Mimura, T. (2004) Isolation of intact vacuoles and proteomic analysis of tonoplast from suspension-cultured cells of *Arabidopsis thaliana*. *Plant Cell Physiol.* **45,** 672–683
34. Carter, C., Pan, S., Zouhar, J., Avila, E. L., Girke, T., and Raikhel, N. V. (2004) The vegetative vacuole proteome of *Arabidopsis thaliana* reveals predicted and unexpected proteins. *Plant Cell* **16,** 3285–3303
35. Dietz, K. J., Tavakoli, N., Kluge, C., Mimura, T., Sharma, S. S., Harris, G. C., Chardonnens, A. N., and Golldack, D. (2001) Significance of the V-type ATPase for the adaptation to stressful growth conditions and its regulation on the molecular and biochemical level. *J. Exp. Bot.* **52,** 1969–1980
36. Cho, Y. H., Yoo, S. D., and Sheen, J. (2006) Regulatory functions of nuclear hexokinase 1 complex in glucose signaling. *Cell* **127,** 579–589
37. Pardee, J. D., and Spudich, J. A. (1982) Purification of muscle actin. *Methods Cell Biol.* **24,** 271–289
38. Pollard, T. D. (1984) Polymerization of ADP-actin. *J. Cell Biol.* **99,** 769–777
39. Yarmola, E. G., Somasundaram, T., Boring, T. A., Spector, I., and Bubb,

M. R. (2000) Actin-latrunculin A structure and function. Differential modulation of actin-binding protein function by latrunculin A. *J. Biol. Chem.* **275,** 28120–28127
40. Huang, S., Blanchoin, L., Kovar, D. R., and Staiger, C. J. (2003) *Arabidopsis* capping protein (AtCP) is a heterodimer that regulates assembly at the barbed ends of actin filaments. *J. Biol. Chem.* **278,** 44832–44842
41. Khurana, P., Henty, J. L., Huang, S., Staiger, A. M., Blanchoin, L., and Staiger, C. J. (2010) *Arabidopsis* VILLIN1 and VILLIN3 have overlapping and distinct activities in actin bundle formation and turnover. *Plant Cell* **22,** 2727–2748
42. Xiang, Y., Huang, X., Wang, T., Zhang, Y., Liu, Q., Hussey, P. J., and Ren, H. (2007) Actin-binding protein 29 from *Lilium* pollen plays an important role in dynamic actin remodeling. *Plant Cell* **19,** 1930–1946
43. Zhao, Y., Zhao, S., Mao, T., Qu, X., Cao, W., Zhang, L., Zhang, W., He, L., Li, S., Ren, S., Zhao, J., Zhu, G., Huang, S., Ye, K., Yuan, M., and Guo, Y. (2011) The plant-specific actin-binding protein SCAB1 stabilizes actin filaments and regulates stomatal movement in *Arabidopsis*. *Plant Cell* **23,** 2314–2330
44. Glenney, J. R., Jr., Kaulfus, P., and Weber, K. (1981) F actin assembly modulated by villin. Ca^{2+}-dependent nucleation and capping of the barbed end. *Cell* **24,** 471–480
45. Walsh, T. P., Weber, A., Higgins, J., Bonder, E. M., and Mooseker, M. S. (1984) Effect of villin on the kinetics of actin polymerization. *Biochemistry* **23,** 2613–2621
46. Pollard, T. D., and Cooper, J. A. (1984) Quantitative analysis of the effect of *Acanthamoeba* profilin on actin filament nucleation and elongation. *Biochemistry* **23,** 6631–6641
47. Holliday, L. S., Bubb, M. R., Jiang, J., Hurst, I. R., and Zuo, J. (2005) Interactions between vacuolar H^+-ATPases and microfilaments in osteoclasts. *J. Bioenerg. Biomembr.* **37,** 419–423
48. Zuo, J., Vergara, S., Kohno, S., and Holliday, L. S. (2008) Biochemical and functional characterization of the actin-binding activity of the B subunit of yeast vacuolar H^+-ATPase. *J. Exp. Biol.* **211,** 1102–1108
49. Cooper, J. A., and Schafer, D. A. (2000) Control of actin assembly and disassembly at filament ends. *Curr. Opin. Cell Biol.* **12,** 97–103
50. Shimmen, T., Hamatani, M., Saito, S., Yokota, E., Mimura, T., Fusetani, N., and Karaki, H. (1995) Roles of actin filaments in cytoplasmic streaming and organization of transvacuolar strands in root hair cells of Hydrocharis. *Protoplasma* **185,** 188–193
51. Winter, D., Vinegar, B., Nahal H., Ammar R., Wilson, G. V., Provart, N. J. (2007) An "Electronic Fluorescent Pictograph" browser for exploring and analyzing large-scale biological data sets. *PLoS One* **2,** e718